33RD INTERNATIONAL COSMIC RAY CONFERENCE, RIO DE JANEIRO 2013
THE ASTROPARTICLE PHYSICS CONFERENCE

Precision measurement of the positron fraction in primary cosmic rays of 0.5−350 GeV

A. KOUNINE[1], ON BEHALF OF THE AMS COLLABORATION[2].

[1] *Massachusetts Institute of Technology, Cambridge, USA*
[2] *for the complete list of the authorts see the AMS Collaboration list (for ID1264) in these proceedings.*

Andrei.Kounine@cern.ch

Abstract: A precision measurement by AMS on the ISS of the positron fraction in primary cosmic rays in the energy range from 0.5 to 350 GeV based on 6.8 million positron and electron events is presented. The very accurate data show that the positron fraction is steadily increasing from 10 to ∼250 GeV, but, from 20 to 250 GeV, the slope decreases by an order of magnitude. The positron fraction spectrum shows no fine structure.

Keywords: Cosmic rays, positron fraction.

1 AMS Detector

The Alpha Magnetic Spectrometer, AMS-02, is a general purpose high energy particle physics detector. It was installed on the International Space Station, ISS, on 19 May 2011 to conduct a unique long duration mission (∼20 years) of fundamental physics research in space. Reported results are based on the data collected during the initial 18 months of operations on the ISS, from 19 May 2011 to 10 December 2012 [1]. This constitutes 8 % of the expected AMS data sample. The positron fraction, that is, the ratio of the positron flux to the combined flux of positrons and electrons, is presented in this article in the energy range from 0.5 to 350 GeV.

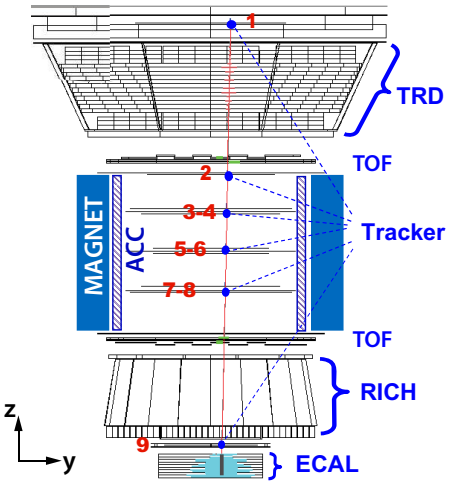

Figure 1: A 369 GeV positron event as measured by the AMS detector on the ISS in the (y-z) plane. Tracker planes 1-9 measure the particle charge (+1) and momentum. The TRD identifies the particle as an electron/positron. The TOF measures the charge and ensures that the particle is downward-going. The RICH measures the charge and velocity. The ECAL independently identifies the particle as an electron/positron and measures its energy.

The layout of the AMS-02 detector [2] is shown in Figure 1. It consists of 9 planes of precision silicon Tracker; a Transition Radiation Detector, TRD; four planes of Time of Flight counters, TOF; a Magnet; an array of anti-coincidence counters, ACC, surrounding the inner Tracker; a Ring Imaging Čerenkov detector, RICH; and an Electromagnetic Calorimeter, ECAL. The figure also shows a high energy positron of 369 GeV recorded by AMS.

There are three main detectors that allow a significant reduction of the proton background in the identification of the positron and electron samples. These are the TRD (above the Magnet), the ECAL (below the Magnet) and the Tracker. The TRD and the ECAL are separated by the Magnet and the Tracker. This ensures that secondary particles produced in the TRD and the upper TOF planes are swept away and do not enter into the ECAL. The matching of the ECAL energy and the momentum measured with the Tracker greatly improves the proton rejection.

The Tracker accurately determines the trajectory and absolute charge (Z) of cosmic rays by multiple measurements of the coordinates and energy loss. Coordinate resolution of each plane is measured to be better than 10 μm in the bending direction and the charge resolution is $\Delta Z \simeq 0.06$ at $Z = 1$. Together with the Magnet, the Tracker provides a Maximum Detectable Rigidity of 2 TV on average [3], over Tracker planes 1 to 9.

The TRD is designed to use transition radiation to distinguish between $e^{\pm}$ and protons, and dE/dx to independently identify nuclei [4]. It consists of 5,248 proportional tubes of 6 mm diameter arranged in 20 layers interleaved with a 20 mm thick fiber fleece radiator. In order to differentiate between $e^{\pm}$ and protons, signals from the 20 layers are combined in a TRD estimator formed from the ratio of the log–likelihood probability of the $e^{\pm}$ hypothesis to that of the proton hypothesis. The proton rejection power of the TRD estimator at 90 % $e^{\pm}$ efficiency measured on orbit is 10^3 to 10^4, as shown in Figure 2a.

The ECAL consists of a multilayer sandwich of 98 lead foils and ∼50,000 scintillating fibers with an active area of $648 \times 648\,\mathrm{mm}^2$ and a thickness of 166.5 mm corresponding to 17 radiation lengths [5]. The calorimeter is composed of 9 superlayers, with the fibers running in one direction only in each superlayer. The 3–D imaging capability of the detector is obtained by stacking alternate superlayers with fibers parallel to the x- and y-axes (5 and 4 superlayers, respectively). The energy resolution of the

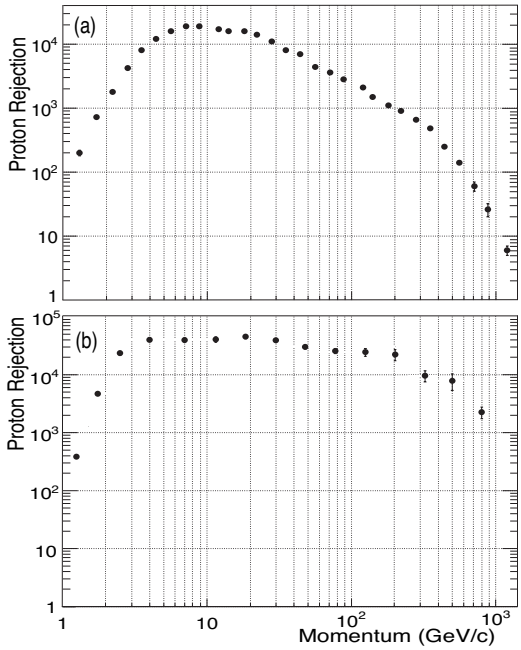

Figure 2: (a) The proton rejection measured by the TRD as a function of track momentum at 90 % selection efficiency for $e^{\pm}$. (b) The measured proton rejection using the ECAL and the Tracker. For 90 % $e^{\pm}$ ECAL selection efficiency, the measured proton rejection is ∼10,000 for the combination of the ECAL and the Tracker in the momentum range 3–500 GeV/c, independent of the TRD.

ECAL is parametrized as a function of energy (in GeV) $\sigma(E)/E = \sqrt{(0.104)^2/E + (0.014)^2}$. In order to cleanly identify electrons and positrons, an ECAL estimator, based on a Boosted Decision Tree, BDT, algorithm [6], is constructed using the 3–D shower shape in the ECAL. The proton rejection power of the ECAL estimator when combined with the energy-momentum matching requirement $E/p > 0.75$ reaches ∼10,000 (see Figure 2b), as determined from the ISS data.

The proton rejection power can be readily improved by tightening the selection criteria with reduced $e^{\pm}$ efficiency.

2 Data sample and analysis procedure.

Over 25 billion events have been analyzed. Optimization of all reconstruction algorithms was performed using the test beam data. Corrections are applied to the data to ensure long term stability of the absolute scales in the varying on orbit environment. These corrections are determined using specific samples of particles, predominantly protons. In addition, stability of the electronics response is ensured by calibrations of all channels every half-orbit (∼46 min).

Monte Carlo simulated events are produced using a dedicated program developed by AMS which is based on the GEANT-4.9.4 package [7]. This program simulates electromagnetic and hadronic interactions of particles in the materials of AMS and generates detector responses. The digitization of the signals, including those of the AMS trigger, is simulated precisely according to the measured characteristics of the electronics. The digitized signals then undergo the same reconstruction as used for the data. The Monte Carlo samples used in the present analysis have sufficient statistics so they do not contribute to the errors.

For this analysis events are selected by requiring a track in the TRD and in the Tracker, a cluster of hits in the ECAL and a measured velocity $\beta \sim 1$ in the TOF consistent with a downward-going $Z = 1$ particle. In order to reject > 99 % of the remaining protons, an energy-dependent cut on the ECAL estimator is applied. In order to reject positrons and electrons produced by the interaction of primary cosmic rays with the atmosphere [8], the energy measured with the ECAL is required to exceed by a factor of 1.2 the maximal Stoermer cutoff [9] for either a positive or a negative particle at the geomagnetic location where the particle was detected at any angle within the AMS acceptance.

The selection efficiency for positrons and electrons is estimated to be ∼90 % in the acceptance of the ECAL. Any charge asymmetry in the selection efficiency, important only at very low energies (below 3 GeV), is accounted for in the systematics. The remaining sample contains ∼6,800,000 primary positrons and electrons and ∼700,000 protons. The composition of the sample versus energy is determined by the TRD estimator and E/p matching.

The positron fraction is determined in ECAL energy bins. The binning is chosen according to the energy resolution and the available statistics such that migration of the signal events to neighboring bins has a negligible contribution to the systematic errors above ∼2 GeV. The migration uncertainty was obtained by folding the measured rates of positrons and electrons with the ECAL energy resolution.

In every energy bin, the 2-dimensional reference spectra for $e^{\pm}$ and the background are fitted to data in the (TRD estimator–log(E/p)) plane by varying the normalizations of the signal and the background. This method provides a data driven control of the dominant systematic uncertainties by combining the redundant TRD, ECAL and Tracker information. The reference spectra are determined from high statistics, clean electron and proton data samples selected using ECAL information and their Monte Carlo simulation. The 2–D positron reference spectra were verified to be equal to the electron reference spectra using the test

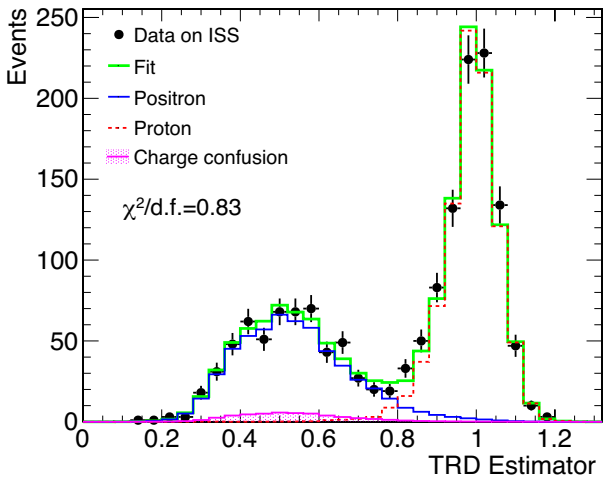

Figure 3: Separation power of the TRD estimator in the energy range 83.2-100 GeV for the positively charged selected data sample. For each energy bin, the positron and proton reference spectra are fitted to the data to obtain the numbers of positrons and protons.

beam data. The fit is performed for positive and negative rigidity data samples yielding, respectively, the numbers of positrons and electrons. Results of a fit for the positive sample in the range 83.2–100 GeV are presented in Figure 3 as a projection onto the TRD estimator axis, where the charge confusion contribution is from electrons misidentified as positrons.

There are several sources of systematic uncertainty including those associated with the asymmetric acceptance of e^+ and e^-, the selection of $e^\pm$, bin-to-bin migration, the reference spectra and charge confusion. The systematic uncertainties were examined in each energy bin over the entire spectrum from 0.5 to 350 GeV.

Two sources of charge confusion dominate. The first is related to the finite resolution of the Tracker and multiple scattering. It is mitigated by the E/p matching and the quality cut of the trajectory measurement. The second source is related to the production of secondary tracks along the path of the primary $e^\pm$ in the Tracker. The impact of the second effect was estimated using control data samples of electron events with the ionization in the lower TOF counters corresponding to at least two traversing particles. Both sources of charge confusion are found to be well reproduced by the Monte Carlo simulation. The systematic uncertainties due to these two effects are obtained by varying the background normalizations within the statistical limits. As an example, for the positive sample in the range 83.2–100 GeV the uncertainty on the number of positrons due to the charge confusion is 1.0 %.

As seen in Figure 3, the proton contamination in the region populated by positrons is small, ∼1 % in this energy range. It is accurately measured using the TRD estimator and therefore has a negligible contribution to the overall error. The systematic error associated with the uncertainty of the reference spectra arises from their finite statistics. It is measured by varying the shape of the reference spectra within the statistical uncertainties. Its contribution to the overall error is small compared to the statistics and is included in the total systematic error.

To evaluate systematic uncertainties related to the selection, the complete analysis is repeated in every energy bin ∼1,000 times with different cut values, such that the selection efficiency varies by 20–30 %. Figure 4a shows the resulting variation of the positron fraction over a range of 83.2-100 GeV. The difference between the width of this distribution from data and from Monte Carlo quantifies the systematic uncertainty due to the selection. Figure 4b shows no correlation between the measured positron fraction and the number of selected positrons.

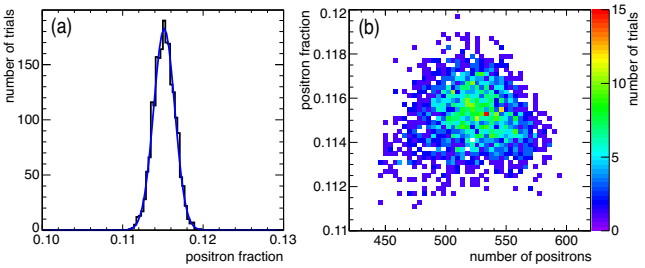

Figure 4: (a) Stability of the measurement in the energy range 83.2-100 GeV over wide variations of the cuts fitted with a Gaussian of width 1.1 %. (b) The positron fraction shows no correlation with the number of selected positrons.

3 Results and conclusions.

The measured positron fraction is presented in Figure 5 as a function of the reconstructed energy at the top of the AMS detector. As seen in the figure, below 10 GeV the positron fraction decreases with increasing energy as expected from the secondary production of cosmic rays by collision with the interstellar medium. The positron fraction is steadily increasing from 10 to ∼250 GeV. This is not consistent with only the secondary production of positrons [10]. The behavior above 250 GeV will become more transparent with more statistics which will also allow improved treatment of the systematics.

The observation of the positron fraction increase with energy has been reported by earlier experiments: TS93 [11], Wizard/CAPRICE [12], HEAT [13], AMS-01 [14], PAMELA [15] and Fermi-LAT [16]. The most recent results are presented in Figure 5 for comparison. The accuracy of AMS-02 and high statistics available enable the reported AMS-02 positron fraction spectrum to be clearly distinct from earlier work (see Figure 6). The AMS-02 spectrum has the unique accuracy and energy range to provide accurate information on new phenomena.

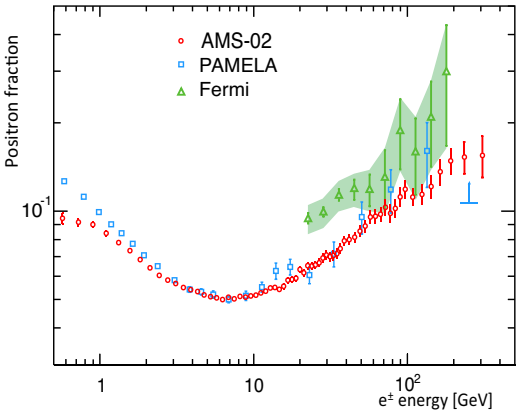

Figure 5: The positron fraction compared with the most recent measurements from PAMELA [15] and Fermi-LAT [16]. The error bars for AMS are the quadratic sum of the statistical and systematic uncertainties and the horizontal positions are the centers of each bin.

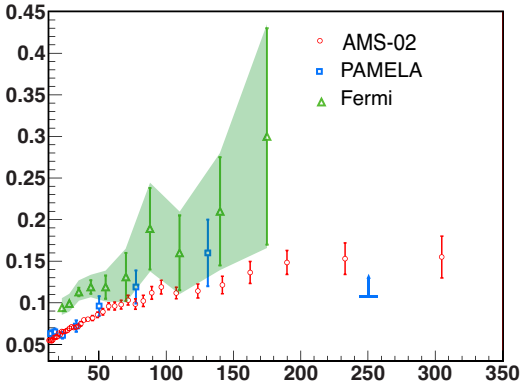

Figure 6: The positron fraction at energies above 10 GeV compared with the most recent measurements from PAMELA [15] and Fermi-LAT [16]. AMS data clearly show the change in the behavior of the positron fraction in this energy range.

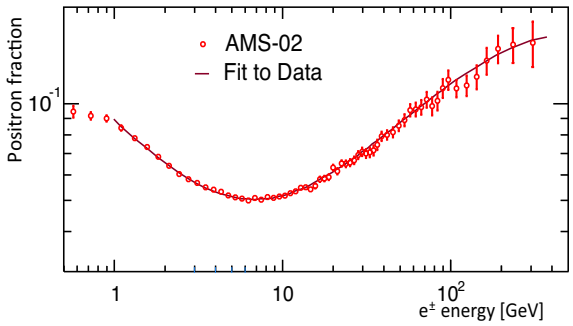

Figure 7: The positron fraction measured by AMS fit with the minimal model. For the fit, both the data and the model are integrated over the bin width. Even with the high statistics and high accuracy of AMS, the spectrum shows no fine structure.

The accuracy of the data enables us to investigate the properties of the positron fraction with different models. We present here the results of comparing our data with a minimal model, as an example. In this model the e^+ and e^- fluxes, Φ_{e^+} and Φ_{e^-}, are parametrized as the sum of individual diffuse power law spectra and the contribution of a single common source of $e^{\pm}$:

$$\Phi_{e^+} = C_{e^+} E^{-\gamma_{e^+}} + C_s E^{-\gamma_s} e^{-E/E_s}; \quad (1)$$

$$\Phi_{e^-} = C_{e^-} E^{-\gamma_{e^-}} + C_s E^{-\gamma_s} e^{-E/E_s}, \quad (2)$$

(with E in GeV) where the coefficients C_{e^+} and C_{e^-} correspond to relative weights of diffuse spectra for positrons and electrons and C_s to the weight of the source spectrum; γ_{e^+}, γ_{e^-} and γ_s are the corresponding spectral indexes; and E_s is a characteristic cutoff energy for the source spectrum. With this parametrization the positron fraction depends on 5 parameters. A fit to the data in the energy range 1 to 350 GeV based on the number of events in each bin yields a $\chi^2/d.f. = 28.5/57$ and $\gamma_{e^-} - \gamma_{e^+} = -0.63 \pm 0.03$, *i.e.*, the diffuse positron spectrum is softer, that is, less energetic with increasing energy, than the diffuse electron spectrum; $\gamma_{e^-} - \gamma_s = 0.66 \pm 0.05$, *i.e.*, the source spectrum is harder than the diffuse electron spectrum; $C_{e^+}/C_{e^-} = 0.091 \pm 0.001$, *i.e.*, the weight of the diffuse positron flux amounts to $\sim$10 % of that of the diffuse electron flux; $C_s/C_{e^-} = 0.0078 \pm 0.0012$, *i.e.*, the weight of the common source constitutes only $\sim$1 % of that of the diffuse electron flux; $1/E_s = 0.0013 \pm 0.0007\,\mathrm{GeV}^{-1}$, corresponding to a cutoff energy of $760^{+1,000}_{-280}$ GeV. The fit is shown in Figure 7 as a solid curve. The agreement between the data and the model shows that the positron fraction spectrum is consistent with $e^{\pm}$ fluxes each of which is the sum of its diffuse spectrum and a single common power law source. No fine structures are observed in the data. The excellent agreement of this model with the data indicates that the model is insensitive to solar modulation effects [17] during this period. Indeed, fitting over the energy ranges from 0.8–350 GeV to 6.0–350 GeV does not change the results nor the fit quality. Furthermore, fitting the data with the same model extended to include different solar modulation effects on positrons and electrons yields similar results. This study also shows that the slope of the positron fraction as a function of energy decreases by an order of magnitude from 20 to 250 GeV.

In conclusion, the first 6.8 million primary positron and electron events collected with AMS on the ISS show: at energies < 10 GeV, a decrease in the positron fraction with increasing energy; a steady increase in the positron fraction from 10 to $\sim$250 GeV; the slope of the positron fraction versus energy decreases by an order of magnitude from 20 to 250 GeV and no fine structure is observed. The agreement between the data and the model shows that the positron fraction spectrum is consistent with $e^{\pm}$ fluxes each of which is the sum of its diffuse spectrum and a single common power law source. These observations show the existence of new physical phenomena. With more data the AMS will be in a unique position to elucidate the nature of these phenomena.

Acknowledgements: This work has been supported by persons and institutions acknowledged in [1], as well as by the Italian Space Agency under contracts ASI-INFN I/002/13/0 and ASDC/011/11/1.

References

[1] M. Aguilar *et al.*, Phys. Rev. Lett. **A 110** (2013) 141102.
[2] A. Kounine, Int. J. Mod. Phys. **E 21** (2012) 123005.
[3] C. Delgado *et al.*, this conference, ID1260.
[4] H. Gast *et al.*, this conference, ID0359.
[5] S. di Falco *et al.*, this conference, ID0855.
[6] B. Roe *et al.*, Nucl. Instrum. Meth. **A 543** (2005) 577.
[7] J. Allison *et al.*, IEEE Trans. Nucl. Sci. **53** (2006) 270; S. Agostinelli *et al.*, Nucl. Instrum. Meth. **A 506** (2003) 250.
[8] J. Alcaraz *et al.*, Phys. Lett. **B 484** (2000) 10.
[9] C. Stoermer, The Polar Aurora, Oxford University Press, London (1950).
[10] P.D. Serpico, Astropart. Phys. **39-40** (2012) 2; T. Delahaye *et al.*, Astron. Astrophys. **501** (2009) 821; I. Moskalenko and A. Strong, Astrophys. J. **493** (1998) 693. We have not included the model predictions as their uncertainty, $\mathcal{O}(20\,\%)$, is larger than our errors. We thank Dr. Moskalenko for useful discussions on this subject.
[11] R. Golden *et al.*, Astrophys. J. **457** (1996) L103.
[12] M. Boezio *et al.*, Adv. Sp. Res. **27-4** (2001) 669.
[13] J. J. Beatty *et al.*, Phys. Rev. Lett. **93** (2004) 241102; M. A. DuVernois *et al.*, Astrophys. J. **559** (2001) 296.
[14] M. Aguilar *et al.*, Phys. Lett. **B 646** (2007) 145.
[15] P. Picozza, "Understanding Cosmic Rays with Balloon and Space Experiments", Proceedings of the 4th International Conference on Particle and Fundamental Physics in Space, Geneva, 5-7 Nov. 2012. The value in the highest energy bin is the 90 % *C.L.* lower limit. We are grateful to Professor Picozza for providing us with accurate information: 1) The PAMELA data are obtained directly from the absolute fluxes of electrons and positrons, gotten independently; 2) The reported errors contain not only statistical errors, but also a portion of the systematics; 3) The data shown have been collected between June 2006 and January 2010. They represent an average of the solar modulation. O. Adriani *et al.*, Astropart. Phys. **34** (2010) 1; O. Adriani *et al.*, Nature **458** (2009) 607.
[16] M. Ackermann *et al.*, Phys. Rev. Lett. **108** (2012) 011103.
[17] I. Usoskin *et al.*, J. Geophysical Research **116** (2011) A02104; Y. Asaoka *et al.*, Phys. Rev. Lett. **88-5** (2002) 051101-1.